Quantum mechanical analysis of fractal conductance fluctuations: a picture using self-similar periodic orbits

2007 J. Phys.: Condens. Matter 19 092002

(http://iopscience.iop.org/0953-8984/19/9/092002)

IOP FTC

IOP PUBLISHING JOURNAL OF PHYSICS: CONDENSED MATTER

J. Phys.: Condens. Matter **19** (2007) 092002 (8pp) doi:10.1088/0953-8984/19/9/092002

FAST TRACK COMMUNICATION

Quantum mechanical analysis of fractal conductance fluctuations: a picture using self-similar periodic orbits

Tatsuo Ogura[1], **Masanori Miyamoto**[1], **Agung Budiyono**[2] **and Katsuhiro Nakamura**[1]

[1] Department of Applied Physics, Osaka City University, Sumiyosi-ku, Osaka 558-8585, Japan
[2] Max Planck Institute for the Physics of Complex Systems, Nöthnitzer Strasse 38, D-01187, Dresden, Germany

E-mail: nakamura@a-phys.eng.osaka-cu.ac.jp

Received 27 October 2006, in final form 22 January 2007
Published 12 February 2007
Online at stacks.iop.org/JPhysCM/19/092002

Abstract

Fractal magnetoconductance fluctuations are often observed in experiments on ballistic quantum dots. Although the analysis of the exact self-affine fractal has been given by the semiclassical theory using self-similar periodic orbits in systems with a soft-walled potential with a saddle, there has been no corresponding quantum mechanical investigation. We numerically calculate the quantum conductance with use of the recursive Green's function method applied to open cavities characterized by a Henon–Heiles type potential. The conductance fluctuations show exact self-affinity just as in some of the experimental observations. The enlargement factor for the horizontal axis can be explained by the scaling factor of the area of self-similar periodic orbits, and therefore be attributed to the curvature of the saddle in the cavity potential. The fractal dimension obtained through the box counting method agrees with those evaluated with use of the Hurst exponent, and coincides with the semiclassical prediction. We further investigate the variation of the fractal dimension by changing the control parameters between the classical and quantum domains.

(Some figures in this article are in colour only in the electronic version)

The recent progress in semiconductor nano-technologies has made it possible to experimentally verify the quantum signature of chaos. Here, the electron mean free path is much longer than the system size with Fermi wavelength less than the characteristic length of devices, and thus the electron transport works in the ballistic and semiclassical domains. The fractal magnetoconductance fluctuation is one of the typical phenomena observed in these experiments. Taylor *et al* fabricated the Sinai billiard at the interface of semiconductor hetero-junctions, and measured the conductance in the weak magnetic field range. The conductance fluctuations showed the exact self-affine fractal in the vicinity of zero magnetic field [1]. In

his pioneering work, Ketzmerick suggested that conductance fluctuations were a fingerprint of the hierarchical mixed-phase-space structure in the underlying classical dynamics [2, 3]. According to this theory, the fractal dimension (D_f) of the statistical fractal-like conductance fluctuations is given by $D_f = 2 - \frac{\gamma}{2}$, where γ is the power of the dwelling time probability, which is assumed to be the same as the distribution of areas enclosed by classical electron trajectories from the entrance to the exit. Since classical dynamics tells us $1 < \gamma < 2$, D_f should take the value $1.0 < D_f < 1.5$. However, most experiments at low temperatures can show D_f larger than 1.5 [4–7]. The experimental results also showed that D_f reaches the maximum in the semiclassical domain, and drops to unity when the system falls in the classical or the quantum domains [5–7]. However, no quantum mechanical investigation has given a satisfactory description of these results.

One way to resolve the above discrepancy and problem is to have recourse to a picture of the self-similar periodic orbits which incorporates contributions of periodic orbits emanating from a saddle of general quantum cavities. In fact, saddles are widely created inside the cavity as a consequence of soft-wall confinement and at the point contact between the attached leads and the cavity. Two of the present authors (Budiyono and Nakamura) applied the semiclassical Kubo formula [8–10] to the system characterized by a Henon–Heiles type potential which generates self-similar classical periodic orbits through a sequence of isochronous pitchfork bifurcations [11, 12] and indicated that fluctuations can show the exact self-affine fractal [13, 14]. In this type of potential, the harmonic saddles with transverse curvature $\omega_\perp^2$ are related to the scaling factor of the successive self-similar periodic orbits. The fractal magnetoconductance fluctuations were shown to have the power spectra of a Weierstrass-like function. It was shown that D_f can take values larger than 1.5, which violates the results predicted by Ketzmerick, but certainly explains much wider experimental results for the quantum dots accompanied by a potential with saddles. However, the quantum mechanical verification of this semiclassical theory has not been performed so far.

In this letter, we show the quantum mechanical conductance by numerically solving the recursive Green's function applied to the quantum cavity with confining potential of Henon–Heiles type, and confirm the validity of the picture based on self-similar periodic orbits. The conductance fluctuations show the exact self-affinity in accordance with the classical scaling law. We also find that D_f can take values $D_f > 1.5$, confirming the semiclassical issue of [13, 14]. The variation of D_f is also studied against both the finite temperature and the ratio of the system size over Fermi wavelength.

First, we will briefly sketch the work of [13, 14] on the fractal conductance fluctuations. In this theory, the Henon–Heiles potential is chosen to describe a typical cavity having saddles. The scaled potential is written as a function of position coordinate as

$$V_{\mathrm{HH}}(x, y) = 6\epsilon^2[\tfrac{1}{2}(x^2 + y^2) + \epsilon(x^2 y - \tfrac{1}{3}y^3)]. \tag{1}$$

$V_{\mathrm{HH}}(x, y)$ has a saddle at $(x_s, y_s) = (0, \frac{1}{\epsilon})$ with its energy being unity and other equivalent ones at $(x_s, y_s) = (\pm\frac{\sqrt{3}}{\epsilon}, -\frac{1}{2\epsilon})$. The transverse curvature of the saddle is given by

$$\omega_\perp^2 = \left.\frac{\partial^2 V_{\mathrm{HH}}(x, y)}{\partial x^2}\right|_{(x_s, y_s)}. \tag{2}$$

The properties of classical dynamics under this potential are well known [11, 12]. Let us focus on the linear mother orbit A which librates between the wall and the saddle (see figure 1). As the energy increases enough towards the saddle energy, the librating orbit A generates satellites of self-similar figure-of-eight periodic orbits with non-vanishing area through a cascade of the successive pitchfork bifurcations, which play an important role in conductance fluctuations.

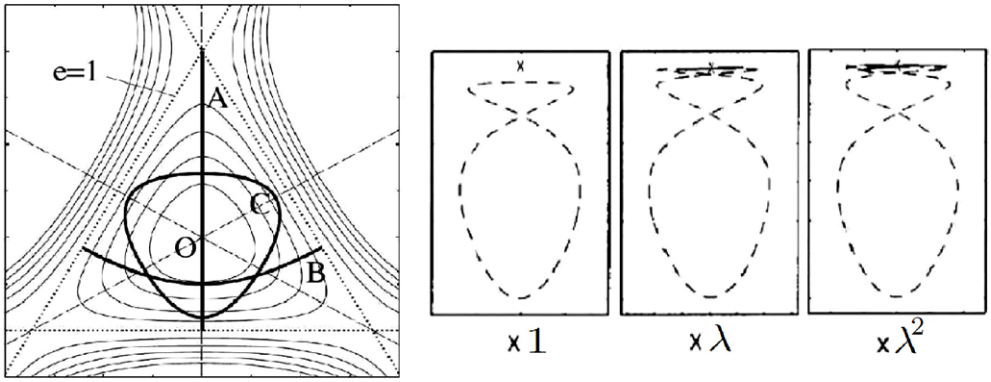

Figure 1. Left panel: Henon–Heiles potential with equi-potential lines and three shortest periodic orbits A, B, and C. O stands for the origin $(x, y) = (0, 0)$. Right panel: self-similar periodic orbits with non-vanishing area generated through orbit bifurcations from orbit A. λ denotes a scaling factor in the text. See [12].

The orbits B and C show no bifurcation and have nothing to do with the fractal. The areas enclosed by the self-similar periodic orbits obey the approximate scaling relation,

$$\Theta_{\rm po}^{(n)} = \lambda \Theta_{\rm po}^{(n-1)}, \qquad 0 < \lambda < 1. \tag{3}$$

Here $\Theta_{\rm po}^{(n)}$ denotes the area enclosed by a periodic orbit born at the nth bifurcation. The scaling factor λ is related to the curvature at the saddle as follows:

$$\lambda = \exp\left(-\frac{\pi}{\omega_\perp}\right). \tag{4}$$

The factor shows up in the exact self-affine conductance fluctuations, which was demonstrated in [13, 14]. In the presence of a weak magnetic field B, one can assume the shape of periodic orbits to be unchanged. Then the action $S_{\rm po}$ evaluated at the Fermi energy $E_{\rm F}$ can be expanded up to the first order in B as follows:

$$S_{\rm po}(E, B) = S_{\rm po}(E, 0) + \frac{e}{c}\Theta_{\rm po} B. \tag{5}$$

The oscillating part of the conductivity can be written in terms of the self-similar periodic orbits in equation (3) [10]:

$$\delta G_{xx}(E, B) = \sum_{\rm po} R_{\rm po}(\tau_\beta) F_{\rm po}(\tau_s) A_{\rm po} \cos\left(\frac{S_{\rm po}(E, 0)}{\hbar} - \frac{\mu_{\rm po}}{2}\pi\right) \cos\left(\frac{e}{c\hbar}\Theta_{\rm po} B\right). \tag{6}$$

$\mu_{\rm po}$ and $A_{\rm po}$ are the Maslov index and the amplitude factor of each periodic orbit, respectively. The temperature T selects only a few shortest periodic orbits that contribute to equation (6) through a damping factor $R_{\rm po}(\tau_\beta) = (T_{\rm po}/\tau_\beta)/\sinh(T_{\rm po}/\tau_\beta)$ with $T_{\rm po}$ the period of periodic orbits and $\tau_\beta = \frac{\hbar}{\pi kT}$ the thermal cut-off. Damping due to a finite mean free path is given by the Born factor $F_{\rm po}(\tau_{\rm s}) = \exp(-T_{\rm po}/2\tau_{\rm s})$, where $\tau_{\rm s}$ is the scattering time. It can be shown that the oscillating part of the conductivity approximately satisfies the following self-affine scaling relationship:

$$\delta G_{xx}(\lambda^{-2} B) \sim \lambda^{-2H(\lambda, T)} \delta G_{xx}(B). \tag{7}$$

This means that the conductivity fluctuations can be rescaled by simultaneously changing the scale of the B-axis (horizontal axis) by $\lambda_B = \lambda^{-2}$ and the scale of the conductivity (vertical axis) by $\lambda_G = \lambda^{-2H}$. $H \equiv \ln \lambda_G / \ln \lambda_B$ is called the Hurst exponent. Using the scaling property

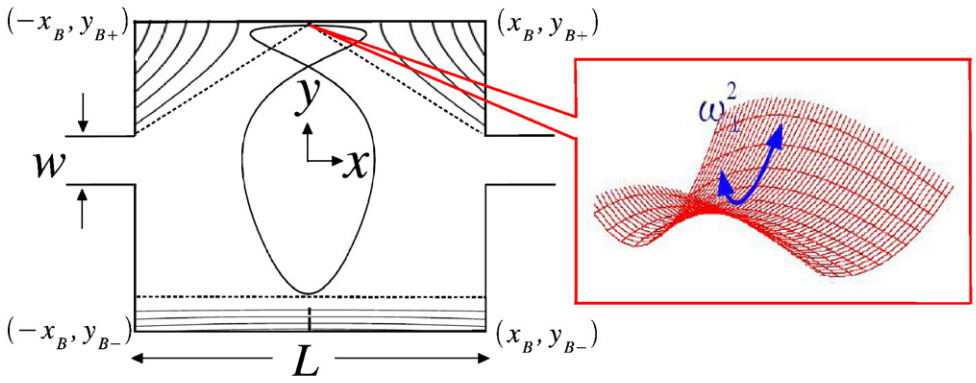

Figure 2. Left panel: the modified Henon–Heiles model and a figure-of-eight periodic orbit. Right panel: a harmonic saddle with curvature $\omega_\perp^2$.

encoded in the Hurst exponent, the fractal dimension of the conductivity fluctuations can then be calculated as $D_f = 2 - H$ with $1 < D_f < 2$ corresponding to $0 < H < 1$ [13, 14].

Our aim is to recover the above exact self-affinity in the quantum mechanical domain. To calculate the conductance for quantum cavities, the recursive Green's function method is employed [15]. To see the self-similar periodic orbits clearly, there is a need to enlarge the scaling factor λ. Therefore, we change the coordinate x into cx, with $0 < c < 1$, to fatten the area of periodic orbits. Accordingly, we employ the following modified model:

$$V(x, y) = 6\epsilon^2(1 - s)E_F[\tfrac{1}{2}(c^2x^2 + y^2) + \epsilon(c^2x^2y - \tfrac{1}{3}y^3)] \tag{8}$$

with $E_S = (1-s)E_F$ the saddle energy, E_F the Fermi energy, and s a filling factor that controls the saddle energy. As the boundary condition, we assume infinite hard walls located at $y = y_{B+}$ and $y = y_{B-}$, where $y_{B+} = 1/\epsilon$ represents the y coordinates of the saddle. If $s(>0)$ comes close to zero, E_S is nearly equal to E_F. Then the suppression of the probability density of the wavefunction around the saddle makes it harder for the important periodic orbits to contribute to the quantum transport. If s becomes too large, on the other hand, the effect of the hard-walled boundary at $y = y_{B+}$ becomes serious and smears out the role of the saddle. Considering the above reasons, we choose $s = 0.1$ to set the case in which the most interesting phenomenon is expected. Despite this modification, the properties of classical dynamics are essentially the same as in the unscaled Henon–Heiles system. Two leads are characterized by the potential, $U_{\text{lead}}(y) = (\Theta(\tilde{y} - \frac{w}{2}) + \Theta(-\frac{w}{2} - \tilde{y}))V_c + \Theta(\tilde{y} + \frac{w}{2})\Theta(-\tilde{y} + \frac{w}{2})V(\pm L/2, y)$ with $\tilde{y} = y - y_0$ and $V_c = 10E_F$, and attached to the right and left sides of the cavity so that the saddle on the middle top is kept away from the leads as in figure 2.

The numerical calculation is performed with the 116×216 lattice and the ratio between the lattice constant a and the Fermi wavelength $a/\lambda_F = 0.197$. We choose the ratio between the characteristic length of the cavity and the Fermi wavelength to be $L/\lambda_F = 22.83$. The mode number is $n = 6$. Then the electron can be considered to be in the semiclassical region. The unitarity precision depends on the nature of evanescent modes included in our numerical treatment. In the presence of field B, the precision (per mode) is stable regardless of the location (y_0) of leads, so long as y_0 falls in the central third in the vertical width between y_{B-} and y_{B+}. However, it becomes unstable when y_0 is close to the upper or lower boundary of the cavity. The latter difficulty is caused by the appearance of the anomalously large vertical evanescent modes in such limiting cases. To keep the stable precision, we have chosen the value y_0 in

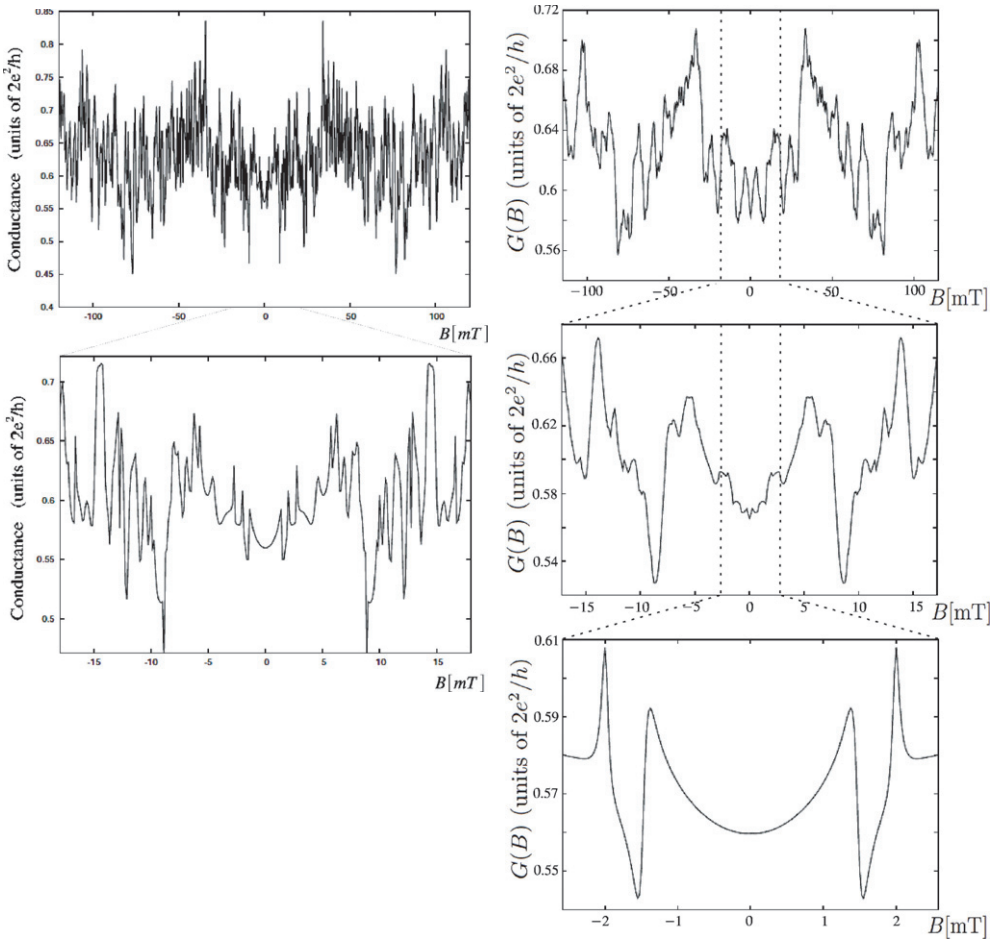

Figure 3. Left panel: numerical results for magnetoconductance fluctuations $G(B)$ and a partial magnification in the case of $\lambda = 0.387$ and $\omega_\perp = 3.31$. Right panel: the successive magnification of the coarse grained conductance fluctuations.

the above central region so as not to meet such anomalous evanescent modes. Figures 3 and 4 show the quantum mechanical conductance as a function of B. The results are obtained under the unitarity precision 1 ± 0.002. At a very few exceptional B values, however, the precision suddenly drops to the level 1 ± 0.02, which does not affect the global structure of curves in figures 3 and 4.

In our model, with use of the effective mass m^* of the electron, the transverse curvature of the saddle is written as

$$\left.\frac{\partial^2 V(x, y)}{\partial x^2}\right|_{(x_s, y_s)} = m^* \omega_\perp^2 = 18\epsilon^2(1 - s)E_F c^2. \tag{9}$$

The left panel of figure 3 shows the self-affine-like structure around $B = 0$. To see the self-affinity more clearly, we perform the coarse graining of the conductance fluctuations. The result is given on the right panel of figure 3. (At the top of the figure, for example, the coarse graining is done by averaging $G(B)$ over each interval of $\Delta B = 5$ mT, with successive intervals chosen by shifting the preceding one by $\delta B = 0.125$ mT.) The magnification factors in the

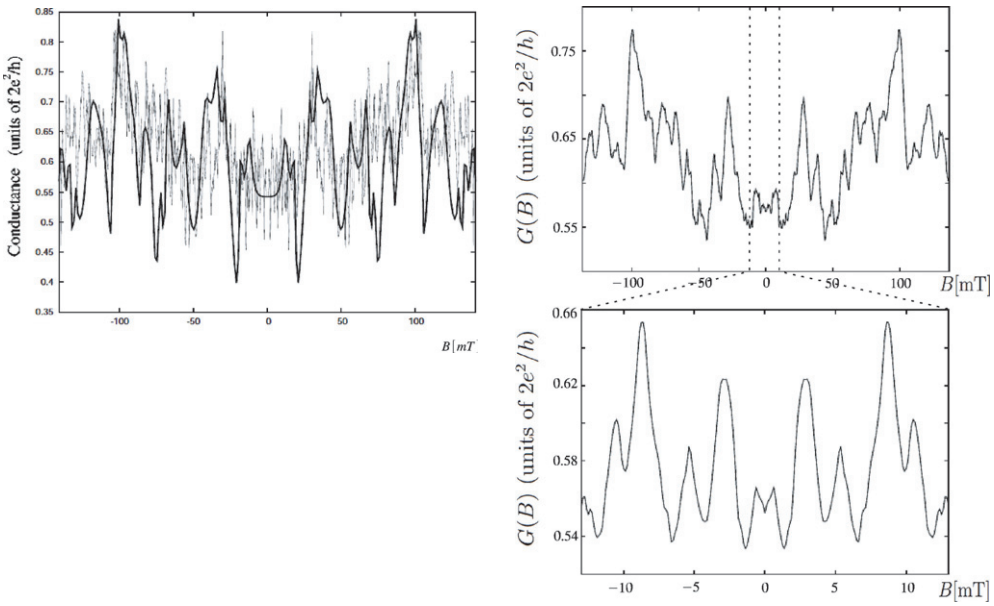

Figure 4. Left panel: quantum mechanical magnetoconductance $G(B)$ in the case of $\lambda = 0.309$ and $\omega_\perp = 2.67$ (thin line). The magnification of the range at -13 mT $\leqslant B \leqslant 13$ mT is given by the bold line. Right panel: a partial magnification of the coarse grained conductance fluctuations.

horizontal and vertical directions are respectively $\lambda_x = 6.68$ and $\lambda_y = 1.8$ (both evaluated from the left panel). The value λ_x turns out to be equal to $\lambda^{-2} = \exp(\frac{2\pi}{\omega_\perp}) = (0.387)^{-2}$ with $\omega_\perp = 3.31$ employed in equation (9). Then the fractal dimension is calculated as $D_\mathrm{f} = 2 - H = 2 - \frac{\ln \lambda_y}{\ln \lambda_x} = 1.69$, which is consistent with that of the semiclassical theory [13, 14]. For comparison, another analysis of D_f based on the box counting method is performed, giving $D_\mathrm{f} = 1.64$. (The power law behaviour can be observed for boxes on scales from $(\delta B, \delta G) = (1.1, 0.004)$ through $(16.2, 0.054)$ in the left panel of figure 3.) This is almost the same value as calculated in terms of the Hurst exponent.

Next, we calculate the magnetoconductance when $\lambda = 0.309$ with a different value of $\omega_\perp = 2.67$ (see figure 4). The self-affinity is shown in two ways as in the case of figure 3. In the left panel of figure 4 the bold line is obtained by partially magnifying the original thin lines by $\lambda_x = \lambda^{-2} = 10.47$ in the x axis and by $\lambda_y = 2.0$ in the y axis. In this choice of λ_x and λ_y, major peaks and dips nicely coincide between the magnified and non-magnified structures. Then, the fractal dimension D_f is equal to $2 - \frac{\ln \lambda_y}{\ln \lambda_x} = 1.70$.

On the other hand, there are experimental studies on the effect of transition from classical (large (scaled) size of the cavity L/λ_F and finite temperature $k_\mathrm{B}T$) to quantum (small L/λ_F and $k_\mathrm{B}T = 0$) limits on D_f, and some experiments indicate $1.5 < D_\mathrm{f} < 1.6$ [5–7]. We therefore investigate the variation of D_f against L/λ_F and $k_\mathrm{B}T$. The finite temperature effect on the conductance is written as

$$\langle G(B) \rangle = \int \mathrm{d}E \left(-\frac{\partial f}{\partial E} \right) G(E, B), \tag{10}$$

where f is the Fermi distribution function. Below, the curvature at the saddle is fixed so that $\lambda = 0.387$ and the box counting method is used. The result is shown in table 1. D_f takes a maximum at the zero temperature under the largest L/λ_F, namely in the semiclassical domain, and drops towards unity when the system falls in the classical and quantum domains.

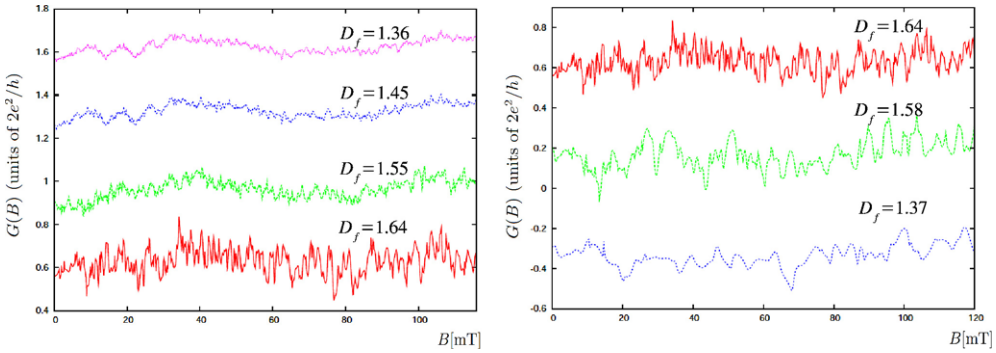

Figure 5. Left panel: the effect of finite temperature k_BT on $G(B)$ and D_f under a fixed $L/\lambda_F = 22.83$. Traces are vertically offset for clarity. From top to bottom: $k_BT/E_F = 0.0591$, 0.0197, 0.00197, 0. Right panel: the effect of L/λ_F on $G(B)$ and D_f under a fixed $k_BT/E_F = 0$. From top to bottom: the $L/\lambda_F = 22.83$, 18.27, 9.13.

Table 1. Variation of fractal dimension.

k_BT/E_F	L/λ_F	D_f
0.0591	22.83	1.36
0.0197	22.83	1.45
0.00197	22.83	1.55
0	22.83	1.64
0	18.27	1.58
0	9.13	1.37

To see this assertion more vividly, we show in figure 5 the T- and L/λ_F-dependence of the spectra. In fact, the enhanced thermal effect (left panel) and the quantum effect (right panel) rapidly suppress the fractal structure. These behaviours are consistent with the experimental results [5–7]. Precisely speaking, the value of D_f becomes difficult to evaluate for high temperatures, since the integration range in equation (10), $|E-E_F| \leqslant k_BT$, becomes broadened as T is increased. While $G(B)$ and D_f at $k_BT/E_F \leqslant 0.02$ in table 1 and figure 5 are converged values, those at $k_BT/E_F = 0.0591$ are not fully converged because the number of the calculated data is still limited. However, the averaging over a sufficiently large number of E-dependent data will smooth out conductance fluctuations, and one can expect a further reduction of D_f in its converged value for $k_BT/E_F = 0.0591$.

In conclusion, by using the numerical quantum mechanical calculation, we have obtained fractal conductance fluctuations in a Henon–Heiles type cavity with attached leads. This potential has harmonic saddles as widely seen in general soft-walled quantum dots, and generates self-similar classical periodic orbits at the saddle through a sequence of pitchfork bifurcations. Our assertion is that fractal conductance fluctuations are caused by this self-similarity of the periodic orbits. Furthermore, the fractal dimension can be larger than 1.5 and coincides with experimental observations. In the present system, although unstable self-similar periodic orbits exist at $E_F > E_S$, the phase space structure can show almost global chaos without island structures. This indicates that the experimental observations of the exact self-affine conductance fluctuations are not the fingerprints of the mixed-phase-space structure, but a general consequence of soft-walled quantum dots with saddles. The reason why other groups failed in obtaining quantum mechanical conductance fluctuations with the fractal dimension larger than 1.5 is that their numerical works were concerned with the confining potential with

no saddle [16–18]. The fractal dimension has a maximum in the semiclassical domain, and drops towards unity when the system falls either in the classical or quantum domains. This behaviour also agrees with the experimental results [5–7]. Although we concentrated on a saddle inside the cavity, those saddles at the point contact between the attached leads and the cavity are found to show the same results as given here, which will be described elsewhere.

The authors are grateful to M Fromhold, H Linke, and Y Ochiai for very useful comments.

References

[1] Taylor R P *et al* 1997 *Phys. Rev. Lett.* **78** 1952
[2] Ketzmerick R 1996 *Phys. Rev.* B **54** 10841
[3] Huckestein B *et al* 2000 *Phys. Rev. Lett.* **84** 5504
[4] Micolich A P *et al* 2000 *Europhys. Lett.* **49** 417
[5] Micolich A P *et al* 2001 *Phys. Rev. Lett.* **87** 036802
[6] Micolich A P *et al* 2004 *Phys. Rev.* B **70** 085302
[7] Bird J P 2003 *Electron Transport in Quantum Dots* (Dordrecht: Kluwer–Academic)
[8] Hackenbroich G and von Oppen F 1995 *Z. Phys.* B **97** 157
[9] Richter K, Ullmo D and Jalabert A 1996 *Phys. Rep.* **276** 1
[10] Nakamura K and Harayama T 2004 *Quantum Chaos and Quantum Dots* (Oxford: Oxford University Press)
[11] Lichtenberg A J and Lieberman M A 1992 *Regular and Chaotic Dynamics* (Berlin: Springer)
[12] Brack M 2001 *Foundation of Physics* **31** 209
[13] Budiyono A and Nakamura K 2003 *Chaos Solitons Fractals* **17** 89
[14] Budiyono A and Nakamura K 2003 *Phys. Rev.* B **68** 121304
[15] Ando T 1991 *Phys. Rev. Lett.* **44** 8017
[16] Takagaki Y and Ploog K H 2000 *Phys. Rev.* B **61** 4457
[17] Tench C R *et al* 2000 *Physica* E **7** 726
[18] Weingartner B, Rotter S and Burgdörter J 2005 *Phys. Rev.* B **72** 115342